A comparative study of the effects of Cu, Rh doping on the microstructure, morphological and optical properties of tin dioxide nanocrystallines

C. X. HU*
The Editorial Department of Journal (Science and Technology) of Shandong University, Southern Campus, Jinan, 250061, People's Republic of China
E-mail: chunxiahu@hotmail.com

Y. S. WU, H. Y. WEI, Y. C. SHI, L. L. WU
School of Materials Science and Engineering, Shandong University (Southern Campus), Jinan, 250061, People's Republic of China

Published online: 5 October 2005

Based on the method of bridging coordinated precursor, pure and Cu, Rh doped tin oxide have been synthesized in order to investigate the influence of metal doping and multi-metal doping on the microstructure and optical properties of the host material. We attest to the formation of a chain-like precursor by FTIR analysis. All the studied systems were characterized by XRD, TEM/HRTEM and UV-VIS. Although Cu doping has few effects on the microstructure, it improves the optical properties of the host material. However Rh doping can apparently affect both the microstructure and the optical property. In the co-doped system, Cu doping reduces the effectiveness of Rh doping greatly.

1. Introduction

Tin dioxide is a wide bandgap material with tetragonal rutile structure (3.6 eV for crystalline SnO_2), used for many applications such as highlight display-technology, solar energy conversion, electrochemical devices and gas sensors, etc. [1, 2]. The knowledge of microstructural properties of nanostructured tin dioxide semiconductor has a fundamental role in the understanding and development of its extended applications.

It is well established that the particle size and microstructrue can affect the properties of nano-scale materials. In some cases, as in optical and electrochemical devices, it is desirable to produce materials with nanometric-scale structures to obtain or improve some specific properties. For tin dioxide system, the ways have been used to improve its some specific properties can be divided into two aspects, using dopants or chosing different preparation methods. Most studies reported in the literature have dealt mainly with the gas sensitivity and conductivity of the tin dioxide doping systems [3] and less care has been devoted to the study of their microstructure and optical parameters. Therefore, this paper is devoted to deal with the doping effects of Cu and Rh metal ions on the microstructure and optical properties of tin dioxide nanocrystalline materials.

2. Experimental details

2.1. Preparation of pure and doping samples

The powders of pure and doped SnO_2 nanocrystallines were synthesized by the method of coordinated precursors [4, 5]. In a typical experimental procedure, $SnCl_2{\cdot}2H_2O$ (Mallinckrodt Baker, USA, purity >99.9%) ethanol solution was first dropped into a cone-beaker. While the cone-beaker was maintained in a water bath of 50°C, the ethanol solution of oxalic acid was then added successively into the above $SnCl_2$ solution. The resulting transparent sol was then added ammonia to keep the solution pH under the condition of pH = 6.75, in order to give enough oxolate anions acting as chelating and bridging ligand. The resulting white gel-like product was then aged for 24 h at 55°C. The resulting precursor was centrifuged, and washed with ethanol by ultrasonic vibration, dried at 60°C for 18 h following by calcinations.

In the case of doping precursors, the ethanol solution of $Cu(NO_3)_2{\cdot}3H_2O$ and $RhCl_3{\cdot}3H_2O$ were added in the $SnCl_2$ ethanol solution for Cu doping and Rh doping samples respectively or added at the same time for Cu-Rh doping one. The procedure then followed was the same as for undoped samples. Based on thermal analysis, the resulting coordinated precursors were

*Author to whom all correspondence should be addressed.
0022-2461
DOI: 10.1007/s10853-005-3139-5

treated in air at 550°C for 4 h with a ramping rate of 3°C/min. All the chemical reagents used in the experiments were purchased from commercial sources and used without further purification.

2.2. Charaterization techniques

Thermoanalysis measurements on the compound precursors were carried out on TG and DSC instruments. All the experiments were carried out between 30 and 830°C at heating rate of $4°C \cdot min^{-1}$ under synthetic air flux.

The investigations of phase and microstructure were carried out using an X-ray diffractometer (Siemens D-5000 instrument using the Ni filtered Cu $K\alpha_2$ radiation), transmission electron microscopy and high resolution transmission electron microscopy analysis (TEM /HRTEM) (Cu10 mol% doping SnO_2 were performed on 200 kV JEOL TEM-2010 ARP; TEM/HRTEM analysis of the other three samples were performed on a

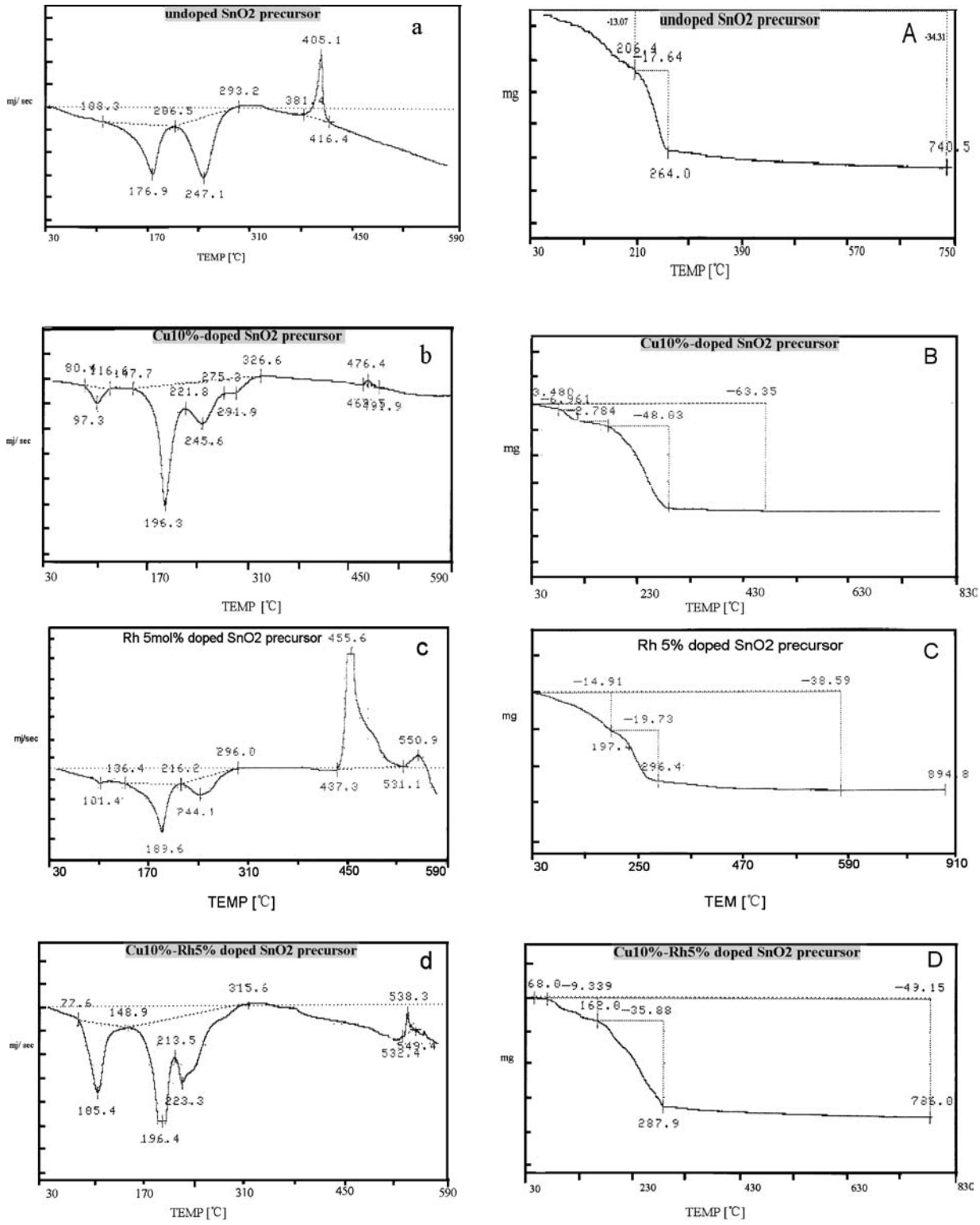

Figure 1 a, b, c and d for the DSC curves of undoped and doped (Cu10 mol%, Rh5 mol%, Cu10-Rh5 mol%) SnO_2 precursors. A, B, C and D for the TG curves of the above four precursors.

Philips U-TWIN TEC NAI 20 operating at an acceleration voltage of 200 kV).

The infrared (IR) spectra of the precursors were measured with BRUKER VECTOR 22 FT-IR. The spectra of the optical transmission of pure and doped SnO_2 over the wavelength region (200–800 nm) were measured in clean air at room temperature by double-beam spectrometer, an SPECORD UV-VIS.

3. Results and discussion

3.1. Thermal analysis

In order to accurately define the temperature at which the crystallization process begins, we have made TG and DSC thermal analyses of the bridging-ligand coordinating precursors. The curves of thermogravimetry and differential scanning calorimetry are shown in Fig. 1. Parts a, b, c and d correspond to the DSC curves of the precursors of pure SnO_2, Cu10 mol%, Rh5 mol% and Cu10-Rh5 mol% doped SnO_2 respectively; parts A, B, C and D refer to the TG curves for the above precursors respectively. All the samples exhibit up to 110°C, an endothermic effect followed by marked mass loss due to the liberation of the physically absorbed water. The amount of the endothermic energy differs for different doping systems. All samples exhibit a continuous mass loss between 108 and 287°C. In this temperature domain, the mass loss (30.71%) of the pure sample is lower than the other three doped ones (57.77% for Cu10 mol% doping sample, 34.64% for Rh5 mol% and 45.22% for Cu10-Rh5 mol% doping ones). Therefore, the metal ions doped precursors loose more weight during the same heat-treatment. The endothermic peaks near 196°C indicates the existence of the organic precursor and the compound formed with sol and organic precursors in the reacting system, which are proved by the FTIR analysis. With increasing temperature, the compounds began to melt and breakaway gradually. Therefore there are no obvious exothermic signals for precursor oxidation in the DSC curves during that temperature range. In spite of that, there is still an obvious trend of weight loss in the TG curve corresponding to slow oxidation. The exothermic peak in the range of 400–500°C (pure sample around 405°C, Cu10 mol% doping around 476°C, Rh5 mol% doping near 455°C and Cu10-Rh5 mol% doping 538°C) is attributed to tin oxide (SnO_2) formation by a complete oxidation process [6]. From the TG curves we can see that all the samples experienced almost no mass loss after 550°C. We attribute this to the crystallisation of the SnO_2. And this can be proved by the following XRD analysis of the 550°C heated materials.

3.2. Microstructure study

Based on the above thermal analysis, we treated the precursors at 550°C in order to obtain the well crystallized samples. Fig. 2 shows the X-ray diffraction patterns of pure and doped SnO_2 samples. The phase of pure and doped materials are not changed and no new phase is observed after heat-treatment, indicating the same rutile lattice structure. The Cu and Rh ions are thought to

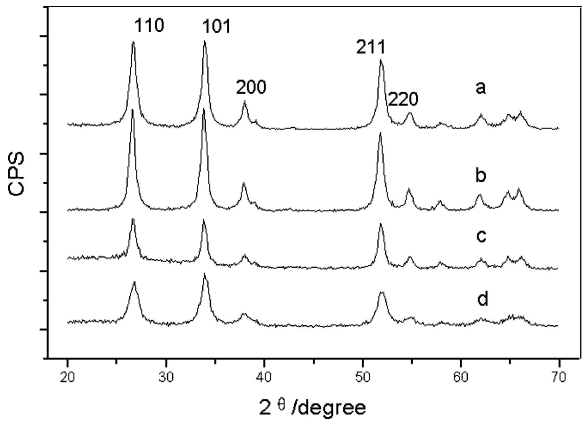

Figure 2 X-ray diffraction patterns for the pure and doped SnO_2 heat-treated at 550°C. (a) for pure SnO_2; b, c and d for Cu10 mol%, Rh5 mol% and Cu10-Rh5 mol% doping material respectively.

be built in onto the lattice site of cation in SnO_2 lattice, thereby acting as dopants. These results are in agreement with other works [7–9] and our following TEM and optical spectrum analysis. The XRD patterns of the pure and doped materials show the presence of SnO_2 peaks corresponding mainly to (110), (101), (211) and (220) lattice planes (Fig. 2). However, the ratio of peak intensities of the doped materials does not correspond to the JCPDS standard data [10]. It can be attributed to the differences (such as the atomic radius and the electronic structure) between the dopant and the host ions. Besides, the destroyed packing caused by the presence of oxygen vacancies in some lattice planes [11] is another important reason. For the doped samples, the crystallinity and particle size of Rh doping materials (Rh5 mol% and Cu10-Rh5 mol%) estimated from the XRD patterns is much lower than the Cu10 mol% doping material. The dopants induced in the prepare procedure cause the appearance of oxygen vacancies in the lattice. The differences of these two metal ions doping will be discussed particularly in the following microstructure analysis. The crystallite sizes obtained by the software of Stokes method (choosing the (110), (101) and (211) lattice planes as the subjects of measurement) are all around 10 nm and decrease in the sequence of Cu10-Rh5 mol% doped SnO_2, undoped SnO_2, and Cu10 mol% doped SnO_2.

The morphology of pure and doped tin oxide nanosized particles is characterized by transmission electron microscopy (TEM) and high-resolution transmission electron microscopy (HRTEM). For the TEM/HRTEM study [12], a drop of the powder suspension is deposited on a carbon-covered nickel grid. Combined with the XRD results (obtained by the software of Stokes method), the doped material presents smaller particle size and crystallite size than the undoped SnO_2. Typical low-magnification HRTEM images of the undoping SnO_2 (Fig. 3(a)) and doping samples (Fig. 3b–d) are shown in Fig. 3. Regular and well-crystallized particles can be observed in all materials. The micrographs are HRTEM images of the pure (Fig. 3(A)) and Cu10 mol%, Rh5 mol% and Cu10-Rh5 mol% doping samples (Fig. 3B–D). It can be observed that the pure SnO_2 had well-defined necks between particles,

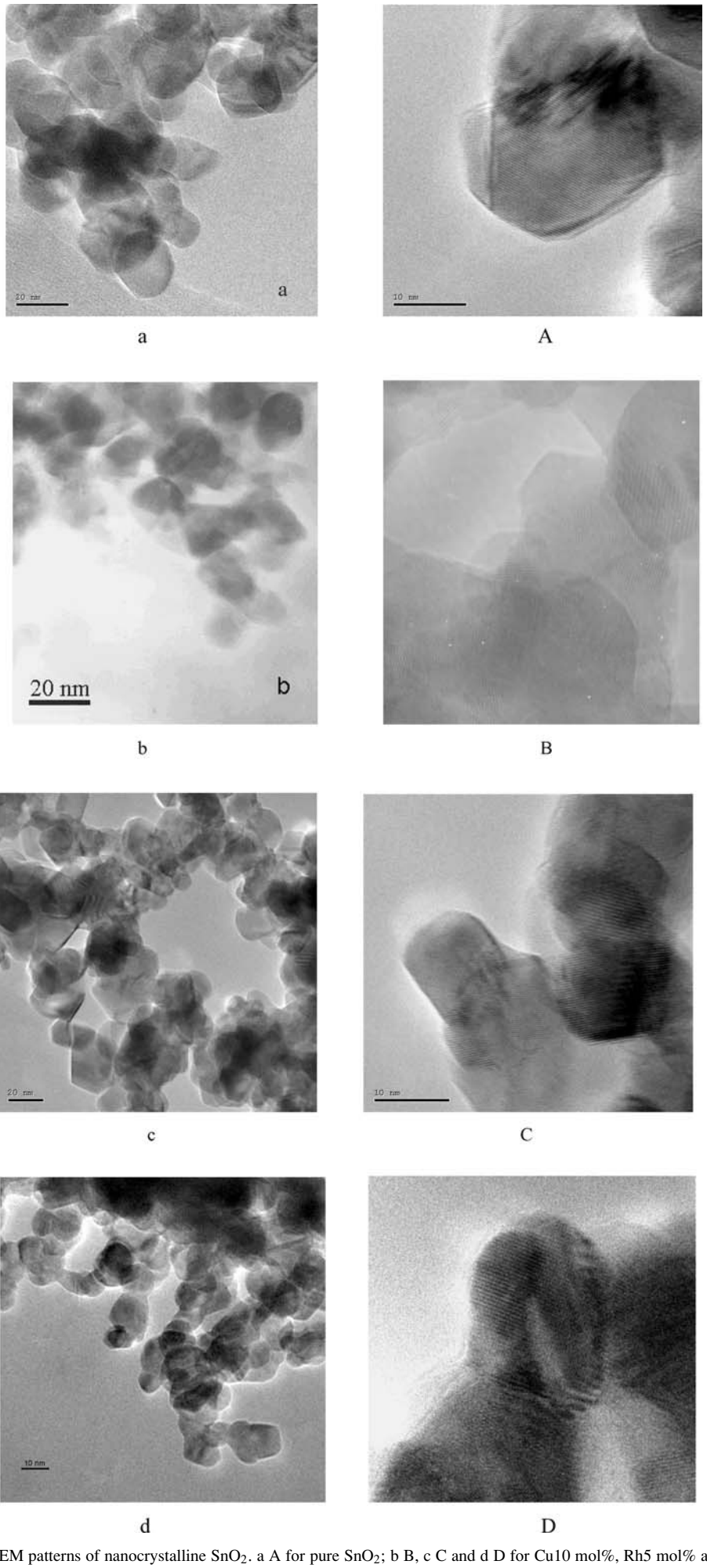

Figure 3 TEM/HRTEM patterns of nanocrystalline SnO_2. a A for pure SnO_2; b B, c C and d D for Cu10 mol%, Rh5 mol% and Cu10-Rh5 mol% doping material respectively.

indicating an advanced stage of particle coalescence. However in the case of doped samples, we find individual particles with a few coalescences. The morphology of pure and Cu doping SnO_2 is almost the same, which means that Cu doping change the particle shape little. However for Rh doping sample, the particles become polygon in shape and the borderline become blur. For the co-doped material, the effect of Cu doping holds back the Rh doping influence. Therefore the co-doped particles become round again and the boundaries get a little clearer than Rh doping samples.

3.3. Optical properties

The FTIR spectra of the precursors taken in the region 4000–400 cm^{-1} provide some information regarding the mode of coordination in the complexes. And the assignment of the featured absorptions attests to the formation of the chain-like coordinated precursors. The most relevant IR absorption bands of the above precursors are shown in Fig. 5. Only the selected infrared bands will be discussed here. References [13, 14] have already reported the IR spectrum data of the oxolate anion acting as the chelating and bridging ligand. The IR spectra of all precursors exhibits two similar types of the coordinating absorption bands, one for bridging ligand at near 1700 and 1440 cm^{-1}, and the other for chelating ligand at near 1640 and 1350 cm^{-1}. All suggesting that the above two coordination types should all exist in those four precursor systems. The possible chain-like structure of precursors is shown in Fig. 4. However there are still some differences among the spectra. For the spectrum of Cu10 mol% doped sample, the absorption around 1400 cm^{-1} changes from a double absorption into a single one, which may correspond to a change of the chelation mode of the oxygen atom in oxalato-bridge (single-dented or double-dented). Cu doping causes to form a few double-dented precursors. However for the Rh doped material, there are no such phenomenon occurs. For Cu10-Rh5 mol% doped precursor, those two particular absorption bands became much weaker and the first band for bridging ligand almost disappeared. We attributed this change to the doping of Cu and Rh at the same time, which may be caused by the differences between these two ions in coordination environments, electronic structure and ion radius. In addition, the vibrations peaks around 750–640 cm^{-1} are assigned to Sn-O vibration according to reference [15] (in the range 500–720 cm^{-1}). However there is no evidence for the existence of absorptions of ν(Cu−O) and ν(Cu−O) [16], which combined with the XRD results prove again that the doping metal ions can only partially take part of Sn lattice site and can not form enough Cu(Rh)−O bonds to be reflected in the IR spectra.

Fig. 6 shows the UV- VIS spectra of ethanol solutions of pure and differently doped tin dioxide nanocrystallines. The UV-VIS spectra of the doping SnO_2 samples are of much difference from the pure one. Comparing to the pure materials, both Cu and Rh doping sample exhibits the higher extremum than the pure one. Therefore the doping of Rh and Cu ions all improves the optical properties of the host SnO_2 material. Moreover, the extremum of Rh doping is the highest in the doped systems and moves toward high wavelength. For the Cu-Rh co-doped system, the extremum is much lower than both Rh and Cu doped samples. Although Cu can increase the extremum of host SnO_2, it holds back the enhancement of Rh doping to the optical extremum when doping with Rh simultaneously. In addition, the sigle peak around 240 nm in Rh doped sample is changed into not only double absorption peak but toward low wavelength in the Cu and Cu-Rh doped systems. The changes are partially caused by the Cu-doping suppression on the optical properties of the host materials. Therefore, the influence of Rh-doping on the optical properties is fully suppressed with the appearance of Cu. Based on detailed analysis, we can conclude that the doping of Cu leads to the disappearance of the

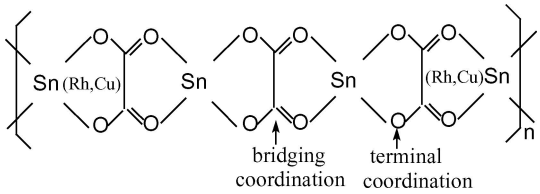

Figure 4 The possible molecular structure of the pure and doping precursors.

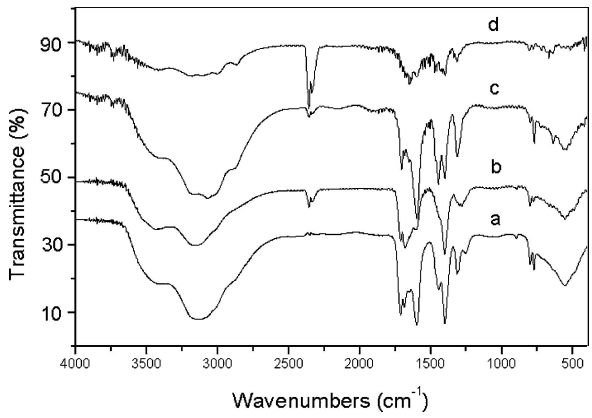

Figure 5 The IR spectra of pure and doped SnO_2 precursors. (a) for pure SnO_2; b, c and d for Cu10 mol%, Rh5 mol% and Cu10-Rh5 mol% doped material respectively.

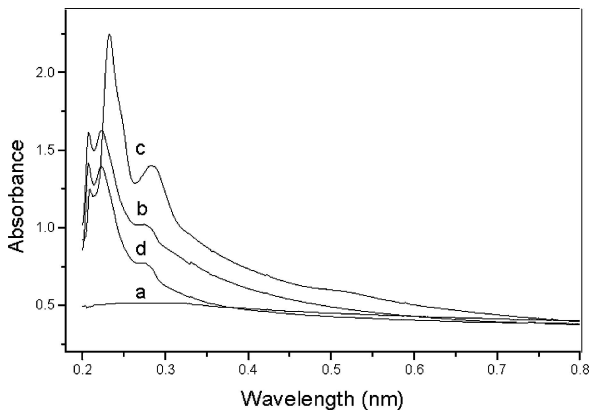

Figure 6 Optical transmission spectra of the pure and doped SnO_2 nanocrystallines. (a) For pure SnO_2; (b), (c) and (d) for Cu10 mol%, Rh5 mol% and Cu10-Rh5 mol% doped material respectively.

optical absorption originated by shallow impurity states [17]. According to reference [17], we assume that the small amount of Cu-dopant leads to more effective localization of free electrons at the surface defects of the host materials. This trait can be explained by lower optical absorption originated by electron transitions from occupied Cu 3d band to the 4s–4p bands when Cu and Rh doping simultaneously. The doping Rh prevents the electronic transition and causing more dislocalization of free electrons. As a result, the Rh doping caused the optical absorption elevated and the optical extremum been much higher than the original SnO_2 materials. Therefore, both Rh and Cu doping have influence on the optical properties of tin oxide. Rh doping has an outstanding ability to improve the optical properties of tin oxide materials. When doping at the same time, Cu doping effect partially cancels the improvement of Rh doping on the optical properties. They restrain the respective doping effects reciprocally. Thereby such Rh doped system can be applied in many fields, such as highlight display-technology.

4. Conclusion

The appearance of typical absorption band of bridging ligand at near 1700 and 1440 cm^{-1}, still the chelating ligand at near 1640 and 1350 cm^{-1}, attests to the formation of our expected coordinating chain-like precursors. This made us find a better way to prepare finely nanocrystallite SnO_2 materials of relatively high optical performance with this low cost and easy handling coordination method.

Comparing to the pure materials, both Cu and Rh doped samples exhibits higher extremum than the pure one. Additionally, the extremum of Rh doping is the highest in the doped systems and moves toward high wavelength. Rh doping has an outstanding ability to improve the optical properties of tin oxide materials. When doping at the same time, effect of Cu doping partially cancels the Rh doping improvement of optical properties. They restrain the respective doping effects reciprocally. This influence is possibly caused by the formation of more effective localized free electrons due to the Cu doping. This agrees well with the XRD and HRTEM analysis and further proves the Rh and Cu doping effects. This confirms that the rarely studied Rh-doping and co-doping system is a promising initial material for producing new optical equipments with high performance, which is the subject of our future work.

Acknowledgements

We acknowledge the help of professor Ning Lun of the Center of HRTEM of Shandong University and professor Jing-Wei Feng of Shanghai Silicate Institute of Chinese Academy of Science in providing TEM and HRTEM data.

References

1. W. A. BADAWAY, *J. Electr. Chem.* **281** (1990) 85.
2. N. MANEVA, K. KYNEV, L. GRIGOROV *et al.*, *J. Mater. Sci. Lett.* **16** (1997) 1037.
3. J. R. YU, G. Z. HUANG and Y. J. YANG, *Sens. Actuat. B* **66** (2000) 286.
4. Y. T. LI, C. W. YAN and C. X. HU, *Polish J. Chem.* **75** (2001) 329.
5. C. X. HU, Z. H. JING and Y. T. LI, *J. Qufu Normal University (Natural Science)* **26** (2000) 68.
6. C. V. SANTILLI, S. H. PULCINELLI and G. E. S. BRITO, *J. Phys. Chem. B* **103** (1999) 2660.
7. E. R. LEITE, J. A. CERRI and E. LONGO *et al. J. Eur. Ceram. Soc.* **21** (2001) 669.
8. I. T. WEBER, R. ANDRADE and E. R. LEITE, *Sens. Actuat. B* **72** (2001) 180.
9. R. MIENTUS and K. ELLMER, *Surf. Coat. Technol.* **98** (1998) 1267.
10. Powder Diffraction File, Data Cards, Inorganic Section, JCPDS, Swarthmore, PA, 1987, 21–1250.
11. K. N. YU, Y. XIONG and Y. LIN *et al.*, *Phys. Rev. B* **55** (1992) 2666.
12. TEM/HRTEM analysis of Cu10 mol% doping SnO_2 were performed on 200 Kv JEOL TEM-2010 ARP; TEM/HRTEM analysis of the other three samples were performed on a Philips U-TWIN TEC NAI 20.
13. D. Z. LIAO, Z. Y. ZHANG and Q. H. ZHAO *et al.*, *J. Chin. Inorg. Chem.* **6** (1990) 193.
14. D. Z. LIAO, J. SHI and Z. H. JIANG *et al.*, *J. Chin. Chem.* **52** (1994) 171.
15. Sadtler Commercial Spectra, IR Grating, INORGANICS, Vol. 1, Y157 O_2Sn.
16. Y. K. KE and H. R. DONG, "The Enchiridion of Analytical Chemistry," 2nd edn (Chemical Industry Press, Pekin, 1998) p. 933.
17. F. CIRILLI, S. KACIULIS, G. MATTOGNO *et al.*, *Thin Solid Films* **315** (1998) 310.

Received 20 May 2003
and accepted 24 March 2005